

HiSST: 4th International Conference on High-Speed Vehicle Science Technology 22 -26 September 2025, Tours, France



Page | 1

Determining the Atomic Arrangement of Disordered Carbon

Lisa A. Price¹, David R. Payne²

Abstract

Disordered carbons, with closed porosity, represent one of the most structurally complex and versatile materials in existence. Their applications are extensive and span a wide range of fields, from Carbon Fibre Reinforced Composites (CFRC) used in the aerospace, automotive and defence industries, to carbon electrodes and semiconductors used in the energy and electronics sectors. Their unique chemical and physical properties are a direct result of their complex microstructures which vary with the method of production, i.e. heat-treatment temperature, heating rate and chemical composition of the organic precursor from which they are formed. Using several advanced x-ray characterisation and electron microscopy techniques at the UK's national synchrotron facility, Diamond Light Source (DLS), we are determining the structure of a series of disordered, porous carbons produced from pyrolysis of phenol-formaldehyde (PF) resins, followed by heat-treatment over a temperature range from 600 to 2800 °C. The experimental results from Raman spectroscopy, Electron Energy Loss Spectroscopy (EELS) and Wide-Angle X-ray Scattering (WAXS) provide detailed information about the local structure and chemical bonding between carbon atoms. At temperatures exceeding 1200°C, there is a noticeable ordering of the atomic structure into coherently scattering nanodomains. With increasing heat-treatment temperature (HTT), sp2 bonded, graphene-like layers extend in directions parallel (La) and perpendicular (Lc) to the plane; La reaches ~70 Å when heated to 2800 °C, with a maximum stack height of Lc ~20 Å, consisting of 6 layers. However, even at the highest HTT of 2800 °C, the atomic structure cannot be reorganised into crystalline graphite; the calculated interlayer distance d(002) remains at 3.45 Å (d(002) for crystalline graphite is 3.35 Å) and the long-range disorder is preserved. It is anticipated that future analysis of data collected from Small-Angle X-ray Scattering (SAXS), ptychography and Coherent Diffraction Imaging (CDI) experiments, in combination with theoretical modelling, will provide further insight into the nanoporosity and micro-structural evolution of these materials as a function of HTT.

Keywords: Disordered Carbon, Atomic Structure, Nanoporosity

Nomenclature

¹ Dstl, Porton Down, Salisbury, Wiltshire, SP4 0JQ, UK, Iprice@dstl.gov.uk

HiSST-2025-185

² Dstl, Porton Down, Salisbury, Wiltshire, SP4 0JQ, UK, DRPAYNE@dstl.gov.uk

BSU - Basic Structural Unit

CDI – Coherent Diffraction Imaging

CFRC - Carbon Fibre Reinforced Composites

DAWN - Data Analysis WorkbeNch

DLS - Diamond Light Source

EDS – Energy Dispersive Spectroscopy

EDX – Energy Dispersive X-ray

EELS – Electron Energy Loss Spectroscopy

FIB - Focussed Ion Beam

FWHM - Full Width Half Maximum

HTT – Heat Treatment Temperature

NGC – Non-Graphitic Carbons

PF – Phenol Formaldehyde

SAXS – Small Angle X-ray Scattering

SEM – Scanning Electron Microscopy

STW - Stone-Thrower-Wales

TEM – Transmission Electron Microscopy

TPS – Thermal Protection Systems

WAXS – Wide Angle X-ray Scattering

XPDF – X-ray Pair Distribution Function

a - interlayer distance

d − Interplanar/Interlayer spacing

f – Atomic scattering factor

F – Structure factor

F(Q) – Reduced Structure Function

G(r) – Reduced PDF

I − Intensity

La – Average graphene intralayer distance

Lc – Average stack height

Lcc - Average C-C bond length

Nc – Number of graphene layers per stack

r – Interatomic distance

Q – Scattering vector

/7− Pi bond

Θ - Scattering angle

 Σ – Sigma bond

l − Wavelength

* – Antibonding

1. Paper content

1.1 Introduction

For more than half a century, carbon materials have been the major constituent for both charring and non-charring ablative thermal protection systems (TPS) for high-speed vehicle structures and rocket propulsion systems. [1,2] This is due to their unique chemical and physical properties, such as low density, high strength to weight ratio and excellent chemical and thermal resistance. These properties are directly related to their complex microstructures; many variations exist, ranging from crystalline diamond and graphite, through all intermediary forms, to amorphous carbon, and each with a unique set of tailored properties. This structural versatility is due to carbon's ability to form sp, sp2 and sp3 bonds via hybridisation of its atomic orbitals. Furthermore, carbon can exist in a number of allotropic crystalline, molecular and metastable forms. [3] Determining the structure of carbon materials at the atomic scale is, therefore, key to understanding and predicting their properties.

Disordered (or "glassy") carbons, with closed nano-porosity, are an important class of sp2-bonded, non-graphitising carbons (NGC). They are formed from pyrolysis of Phenol Formaldehyde (PF) resins, and other similar thermoset polymers, that comprise a high degree of crosslinking and undergo solid-phase carbonisation. Other atoms, such as hydrogen, oxygen and nitrogen, are progressively removed from the polymer network with increasing heat-treatment temperature (HTT); at very high temperatures, a material of greater than 99% carbon content can be produced. However, even after heating to temperatures above 3000 °C, these carbons cannot be fully transformed into crystalline graphite and the amorphous nature of the resin is still reflected in the highly disordered, long-range structure of the heat-treated material. Furthermore, different precursor materials do not undergo the same transformation mechanisms and the structure of the final carbon material is highly dependent on the chemical composition of the starting material and on the processing conditions. This can lead to subtle variations in the spatial arrangement of the carbon atoms which can be detected by diffraction and spectroscopic methods. [4]

Great advancements have been made over the last 70 years in elucidating the structure of non-graphitic carbons (NGCs), with the aim of understanding their structure, properties and resistance to graphitisation. Many proposed models exist, the first of which were proposed by Warren and Rosalind Franklin in the early 1940/50s. [4-5] The short-range structure of these carbons is often described as being turbostratic; planar, sp2-bonded graphene sheets are locally stacked but randomly arranged by rotation perpendicular, and/or displacement parallel, to the plane. These small graphitic domains are limited in extent; typically four or five-layer stacks of nanometre dimensions. This is confirmed by x-ray diffraction patterns which show characteristic broad, unsymmetrical peaks indicating very little three-dimensional crystallinity. Oberlin's model also describes 'basic structural units' (BSUs) which are small graphitic domains with diameters of approximately 1–2 nm. Graphite formation is inhibited by

the random orientation of the BSUs and the presence of cross-links. [6-7] A limitation of both of these models is that they do not specify the nature of the cross-links and, therefore, cannot explain the difference between graphitising and non-graphitising carbons. Jenkins proposed a network of curved and twisted graphene ribbons enclosing irregularly shaped pores that forms from partial preservation of the polymeric precursor after pyrolysis. These ribbons are described using the intra and interplanar parameters, *La* and *Lc*, respectively. However, this relatively open structural model cannot explain the impermeability of the pores to gases. [8]

More recently, it has been shown that the graphene sheets in disordered carbons are not always planar. This is due to the presence of stable five and seven membered rings and Stone-Thrower-Wales (STW) defects. This led to the 'Harris model' consisting of discrete fragments of curved, single-layer graphene sheets, containing both pentagons and heptagons, dispersed throughout a hexagonal network. Harris found evidence for these fullerene-like structures in high-resolution transmission electron microscopy (HRTEM) images. [9]

More exotic molecular carbon structures have also been investigated, including Buckminsterfullerene (C60), carbon nanotubes, nanoonions and nanohorns. [10-12]

There has been considerable research into disordered carbon materials, yet their structures at the atomic scale remain elusive and none of these models have received universal acceptance. This is because disordered carbons are structurally very complex. Investigating these materials at such small, atomic scales presents huge technical challenges. Conventional analytical techniques, such as x-ray diffraction, are limited in their ability to characterise such disordered materials, with a lack of long-range atomic ordering, and particularly those made from light elements such as carbon. The result to date has been an incomplete or simplified description of the microstructure that is heavily built upon assumptions. In addition to determining the atomic arrangement, understanding the origin of the closed porosity, and determining the volume fraction, pore size and geometry, is also of great interest.

This work is part of an ongoing research study to further our understanding of precursor-processing-structure-property relationships of disordered carbons. In particular, we aim to investigate:

- How the structure and chemical composition of the starting polymer affects the structure and properties of the resulting disordered carbon material.
- The mechanism by which the structure of disordered carbons formed from PF resins transform upon increasing HTT.
- The presence of topological defects and curved graphene-like layers.
- The mechanism of pore formation.
- How the structure and porosity of disordered carbons affect thermal transport mechanisms.

To do this, we are carrying out multi-scale testing using a combination of advanced characterisation techniques at the UK's national synchrotron, Diamond Light Source (DLS). Raman spectroscopy, Electron Energy Loss Spectroscopy (EELS) and Wide-Angle X-ray Scattering (WAXS) provide detailed information about the local structure and chemical bonding between carbon atoms, whilst Small-Angle X-ray Scattering (SAXS), ptychography and Coherent Diffraction Imaging (CDI) experiments provide insight into the nanoporosity. Future work will involve generating realistic atomic models of disordered carbons as a function of temperature which will be used to support molecular modelling and calculations of thermal properties.

1.2 Experimental

The disordered carbon samples were prepared from pyrolysis and carbonisation of a PF resin under an inert, argon gas flow at a heating rate of 1 °C /min to 600 °C, where the temperature was held for 1 hour. The samples were further heat-treated to the following temperatures at a heating rate of 5 °C /min; 800, 1200, 1600, 1800, 2000, and 2350 °C. The samples were held at the maximum temperatures for 1 hour. Additional samples were heat-treated to 2600 and 2800 °C under the following conditions: Heating rate 1: Room Temperature (RT) to 1100 °C at 5 °C /min, 1150 to 2600 °C at 2 °C /min, 2600 °C plateau for 60 mins, 2600 °C to RT at 5 °C /min. Heating rate 2: RT to 1100 °C at 5 °C /min, 1150 to 2600 °C at 2 °C /min, 2600 °C at 2 °C /min, 2800 °C plateau for 10

mins, 2800 °C to RT at 5 °C /min.

The heat-treated disordered carbon samples are labelled according to the HTT: HT600, HT800, HT1200, HT1600, HT1800, HT2000, HT2350, HT2600 and HT2800. The cured phenolic resin is labelled as PF and a commercial vitreous carbon as VC.

The normalised mass loss was determined from the change in mass between the post-cured resin and final heat-treated samples. Densities were calculated using the mass and dimensions of the solid samples, shown in Figure 1a.

Elemental analysis was carried out using a ZEISS EVO 25 Scanning Electron Microscope equipped with an Energy Dispersive Spectroscopy (EDS) Oxford Instruments XMax 80 detector running on AZTec software.

Samples were powdered using an automated mortar and pestle. Thin films of < 80 nm were prepared using the E01 JIB 4700F Focused Ion Beam (FIB) and Scanning Electron Microscope (SEM) at the electron Physical Science Imaging Centre (ePSIC), DLS, shown in Figures 1b and 1c.

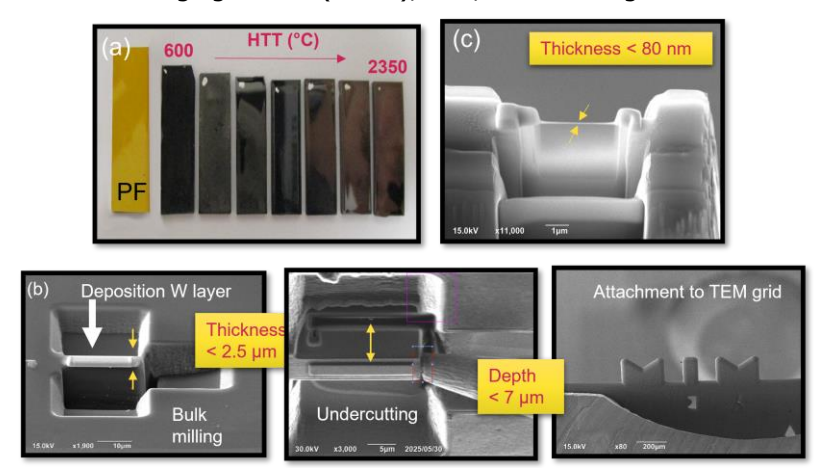


Fig 1. Sample preparation: anticlockwise from (a)-(c); (a) PF resin (yellow) and carbonised samples (black) that have been heat-treated in an inert atmosphere from 600-2350°C (b) FIB lamella preparation and (c) EELS sample < 80 nm thick.

X-ray total scattering measurements were collected on the automated X-ray Pair Distribution Function (XPDF) beamline, I15-1, at DLS, using an X-ray energy of 76.7 keV ($\lambda = 0.161669 \text{ Å}$), with a Q_{max} of 40 Å⁻¹. The powder samples were measured at room temperature in fused quartz (SiO₂) capillaries, with an inner diameter of 0.8 mm and wall thickness of 0.1 mm. Samples were spun at 100Hz with an exposure time of 720 seconds for each measurement. The scattered X-ray radiation was recorded as a two-dimensional diffraction pattern and converted into a one-dimensional function of intensity versus the scattering vector, I(Q), using the DAWN (Data Analysis WorkbeNch) software [13]; Q is the magnitude of the scattering vector $Q = 4\pi \sin\theta/\lambda$, θ is half the scattering angle (2 θ) and λ is the xray wavelength. The total scattering data was reduced into the differential scattering cross-section using the GudrunX software package. [14] Instrument and sample backgrounds were removed and corrections were made for X-ray polarisation, attenuation, multiple scattering and single-atom scattering (including incoherent Compton scattering). Data were normalised to an absolute scale using the Krogh-Moe and Norman method. Diffraction data were then expressed as the structure factor, F(Q) = Q(S(Q) - 1), which is related to the corrected and normalized (to the electron units) intensity, I(O), divided by square of the carbon atomic scattering factor f^2 . Finally, structure factor data F(Q) were converted by the Fourier transform into the real-space, pair distribution functions (PDF), G(r). In the absence of a constraining structural model, peak extraction and peak fitting of PDF data was carried out using the DiffPy SrMise tool. [15] A Gaussian profile was used with a full width half maximum (FWHM) of 0.7 and the PDF backgrounds were estimated using the Fityk programme. [16]

Small Angle X-ray Scattering (SAXS) data were collected using the high-flux, high-resolution, I22 multipurpose SAXS/WAXS beamline at DLS at 18 keV. A Pilatus P3-2M WAXS detector was placed at 0.17 m from sample and a Pilatus P3-2M SAXS detector at ~ 9.7 m from sample. SAXS data are

currently being analysed using the SASView software. [17]

EELS data were collected using the E01 JEOL ARM200CF Microscope with a GIF Continuum K3 (Gatan) EELS spectrometer and K3 (Gatan) detector at ePSIC, DLS. EELS spectra were acquired at 80 keV in STEM (convergent electron beam) mode. This low acceleration voltage was applied to reduce any structural damage of the material that may be caused by the electron beam. Spectra were obtained by integrating multiple pixels from spectrum images (EELS and Energy Dispersive X-ray Spectroscopy (EDX) spectrum images acquired simultaneously) to enhance their signals. The fitting procedure of EELS bands was performed with Fityk software. [16]

Raman Spectra were collected using a Snowy Range Instruments IM-55 785 nm Raman microscope, with an integrated camera. A 3 second integration time was used for all samples. The fitting procedure of the Raman bands was performed with Fityk software. [16]

2. Results and Discussion

2.1 Density and Elemental Analysis

Figure 2 shows the variation in density and carbon content (%) of the samples as a function of HTT. The low densities (significantly less than that of perfect graphite ~2.26 gcm⁻³) are in good agreement with those reported in the literature for NGCs and are a direct consequence of the disordered, highly microporous structure. In comparison to the density of graphite, it can be approximated that a third of the structure is comprised of pores. Studies in the literature have shown that these are closed, nanosized pores (< 2 nm) that are impermeable to gases. [18] The density of the precursor resin is 1.292 gcm⁻³. At low HTTs, low molecular weight gases are evolved, which creates porosity within the sample causing the density to decrease up to 600 °C. Conversely, at higher HTTs, polymeric condensation forms a glassy carbon structure. Gases can then pass through pre-existing pores and chemical densification becomes the predominant effect, resulting in an increase in density up to 1000 °C. Above 1000 °C, the density decreases again due to structural rearrangement and the formation of a large degree of closed porosity. This is typical of NGCs and could indicate the formation of a closed, fullerene-like structures. Figure 2 also shows the percentage carbon content of the samples, as determined by EDX. The composition reaches nearly 100% carbon at the highest HTTs. There is the possibility that some other atoms, such as hydrogen, nitrogen and oxygen, are present in small amounts. However, it is assumed that these are progressively removed with heat treatment temperature, as is well documented in the literature.

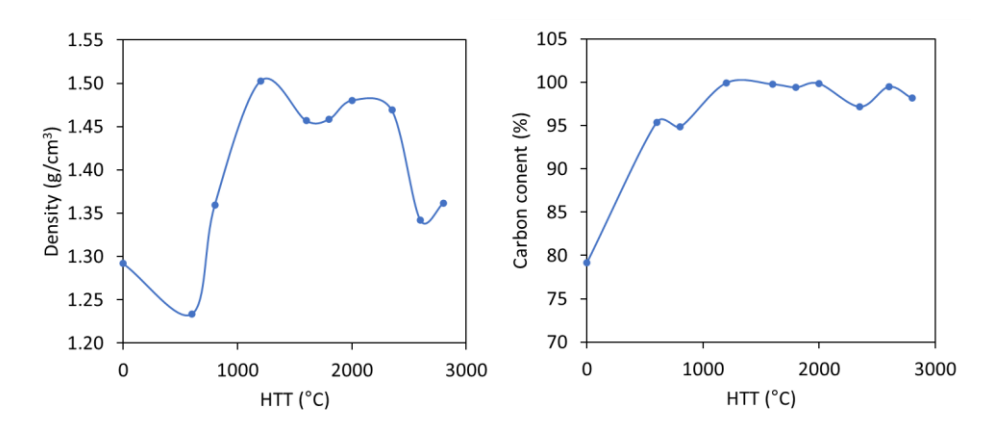


Fig 2. Plots of density and carbon content as a function of HTT.

2.2 WAXS and XPDF

Figure 3 shows the WAXS data set collected on the I15-1 beamline at DLS. The diffraction pattern for the PF resin shows a broad peak at a Q value of $\sim 2~\text{Å}^{-1}$, which is due to adjacent chains of linear polymers. After heat-treatment, the diffraction patterns are consistent with those of typical turbostratic carbons reported in the literature. [2,5,19-23] Figure 3a shows the development of graphite-like 002/reflections (labelled in red) and broad, asymmetric, two-dimensional hk reflections

(labelled in black). The position and width of the 002/ peaks are related to correlations between graphene-like layers and can provide information on structural disorder and stacking heights. The positions and intensities of the hk reflections arise from intralayer correlations and can indicate distortions or defects within the hexagonal rings. The absence of hk/ reflections is due to translational and rotational disorder of the graphene stacks perpendicular to the layer plane, which leads to a lack of three-dimensional periodicity. It has also been suggested that an increase in the degree of curvature of graphenic layers corresponds to an increase in the FWHM of the diffraction peaks. [24] With increasing HTTs, the 002/ and hk reflections become more intense and their peak widths get narrower as the atomic structure becomes more ordered. Figure 3b shows the 002/ peak shifts toward higher scattering angles (smaller d-spacing) as the temperature is increased from 600 - 2800 °C. This is caused by a decrease in the interlayer spacing between adjacent graphene sheets. The peak profile for the 10 reflection also becomes more asymmetric after 1200 °C, however, no peak-splitting to the characteristic 100 and 101 peaks of crystalline graphite is observed. These results provide evidence of a two-dimensional structure, even at the highest HTT of 2800 °C, and confirm resistance to graphitisation.

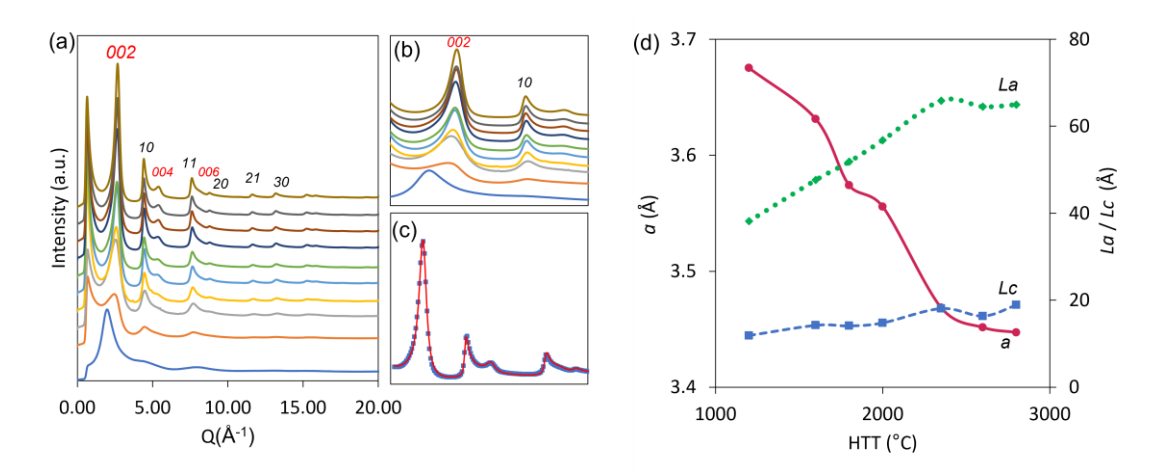


Fig 3. WAXS data set from I15-1 beamline at DLS: from left to right; (a) WAXS data for PF resin (bottom blue trace) and disordered carbons at increasing HTTs from 600-2800 °C (HT600-HT280 bottom to top trace). Interlayer reflections (002/) are labelled in red and asymmetric intralayer *hk* reflections are labelled in black. (b) 002/ and 10 graphite-type reflections increase in intensity and the 002/ peaks shift toward higher scattering angles (smaller *d*-spacing) as the temperature is increased. (c) Refined WAXS profile for HT2800. Blue circles show experimental data and red line shows the resulting peak fit using OctCarb [19]. (d) Nanotextural parameters calculated from refined profiles are plotted showing the layer coherence *La* and stack heights *Lc* increasing with HTT, along with a decrease in interlayer spacing, *a*.

Nanotextural parameters describing the average layer extension (La), stacking height (Lc) and interlayer distance (a) have been extracted from refined profile functions for the (002t) interlayer and (t) intralayer reflections of synchrotron WAXS data using the octave refinement script, OctCarb. [19] Figure 3d summarises the results obtained for samples heat-treated from 1200 – 2800 °C and shows the evolution of structural coherence with HTT. The HT600 and HT800 diffractograms have been omitted from the calculations. Peak fitting of experimental data for these samples was insufficient to provide a good level of confidence in the results due to the large FWHM and overlapping reflections. Both t0 and t0 increase with HTT; the graphene-like sheets extend to ~70 Å, with a maximum stack height of ~20 Å, consisting of 6 layers. The value of the interlayer distance t0 and t0 increase from 3.68 Å at 1200 °C to 3.45 Å at 2800 °C. Although the heat-treated carbons have disordered structures in the long-range, they do possess some distinct structural motifs. An increase in the pyrolysis temperature leads to a noticeable ordering of coherently scattering domains in directions parallel and perpendicular to the graphene layers. However, the general type of disorder is preserved, with the interplanar spacings for all samples being significantly greater than that of crystalline graphite (3.35 Å), even at the highest HTT of 2800 °C. The slower increase of t0 in

comparison to La is further confirmation of the resistance to 3D stacking. These results are consistent with those reported in the literature for heat-treatment of phenolic resins to form carbon structures with imperfect layers of nano-dimensions. The intense peak at very low Q shown in Figure 3a is due to small angle scattering from the variation of electron density with the samples. The scattering intensity at very small angles is the result of inhomogeneity in the sample, such as voids, typically on a scale of 1-100 nm. This is consistent with Franklin's observations of porosity for NGCs. [4] This peak is very small for the PF resin and increases in intensity with increasing HTT.

The experimental WAXS data in form of the structure factors S(Q) and the pair distribution functions G(r) are shown in Figure 4. The sharper peaks at low interatomic distances, r, are due to the intralayer correlations, i.e. coherent scattering domains. The point at which the PDF signal damps to zero intensity provides an indication of the degree of structural coherence. For HT600, broad diffraction peaks are visible in the S(Q) data, and the corresponding PDF exhibits features in a limited range up to 10 Å, indicating the presence of only short-range order in the structure. The PDF plot for the material prepared at 2800 °C shows that the structural coherence extends to approximately 40 Å.

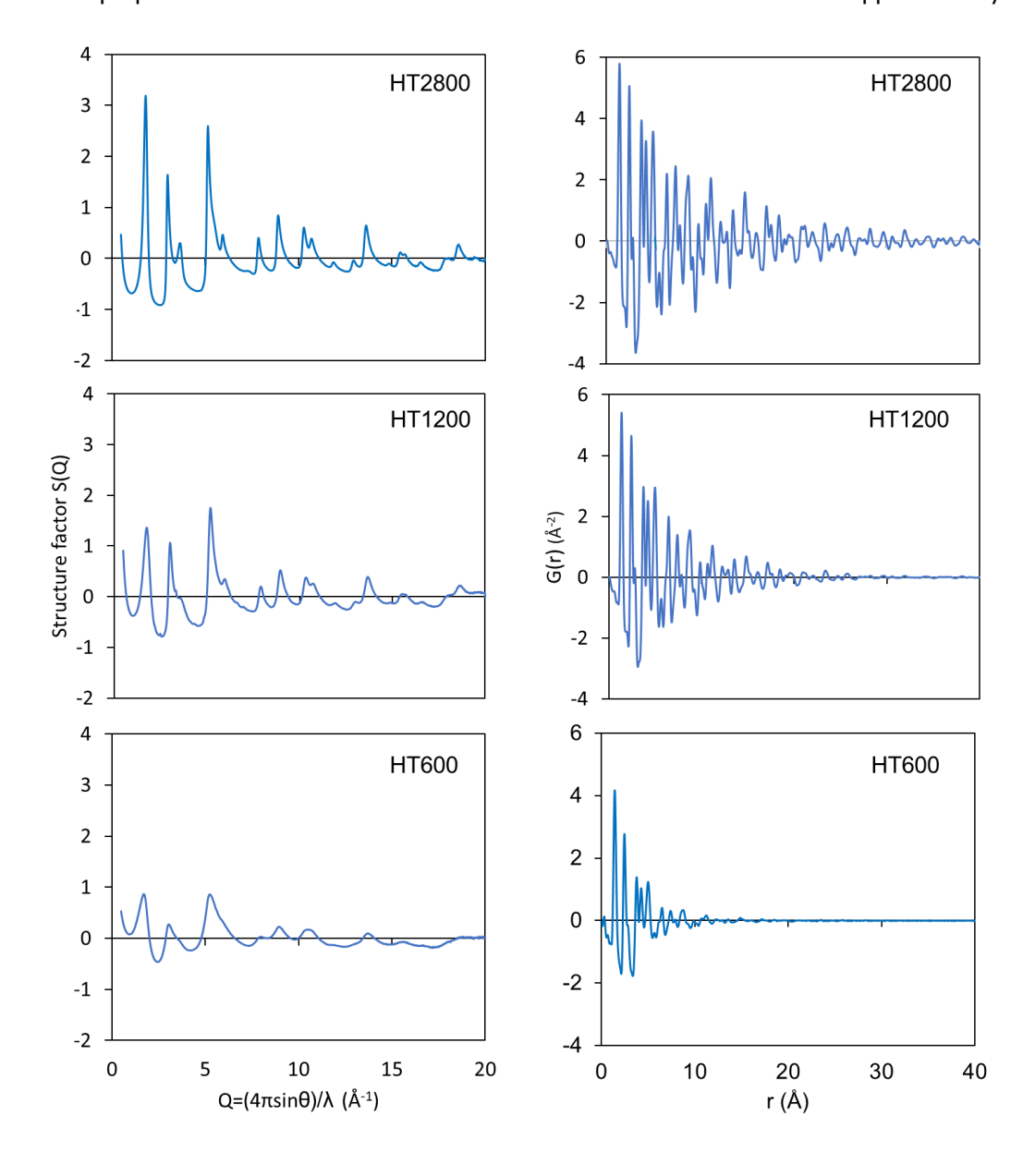


Fig 4. Synchrotron x-ray scattering data from I15-1 beamline at DLS; Experimental structure factors S(Q) and the pair distribution functions G(r) for disordered carbons at increasing HTTs (HT600, HT1200 and HT2800)

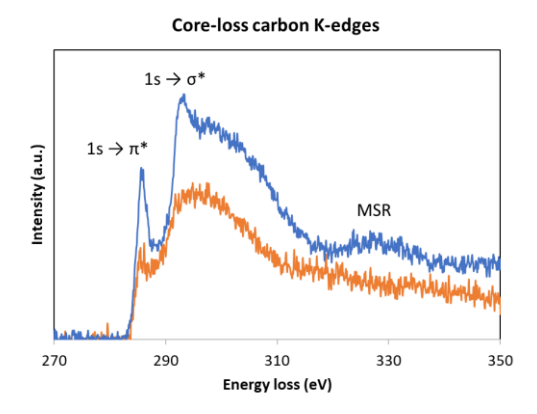
Peak extraction and peak fitting of XPDF data was carried out using the DiffPy SrMise tool. [15] The experimental interatomic distances were obtained from the positions of peak maxima. The first three PDF peaks are positioned at real space distances of \sim 1.41, 2.45, and 2.85 Å match the in-plane carbon–carbon bond distances in the hexagonal, aromatic 6-membered rings of graphite. The width of the peaks represent the probability distributions for the interatomic distances associated with given atom-pairs. Comparing the third peak at $r\sim$ 2.8 Å for the lowest and highest heat-treated samples, we can see that it is much broader and lower in intensity for HT600. The FWHM of this peak decreases with HTT. This has been reported in the literature as strong evidence that there is a significant proportion of non-hexagonal rings in the structure; the third neighbour peak is present in six-membered carbon rings but not in five-membered rings. This has lead to the conclusion that glassy carbon obtained at lower HTTs are composed of curved and defective graphene sheets, whereas carbons pyrolysed at greater than 1200 °C are made of stacks of uncorrelated graphene sheets forming nanocrystalline domains. As the carbonisation process proceeds with increasing HTT, the graphene-like planes grow and rearrange to more ordered structural domains. However, it is apparent that the carbon samples remain non-graphitising up to 2800 °C.

2.3 EELS

Figure 5 shows EELS spectra for the HT800 and HT2000 samples. Two regions of the EELS spectra were acquired for each specimen, the low-loss region (valence excitation spectra, between 0 and 100 eV) and the high-loss (or core-loss) region (between 200 and 500 eV corresponding to excitation of electrons from the core 1s orbital). Two main features are observed in the carbon K-edge region: a $1s\rightarrow \pi^*$ peak at 285 eV, from transitions to unoccupied, antibonding π^* -states, followed by a $1s\rightarrow \sigma^*$ peak at 290 eV and above, from transitions to antibonding, σ^* -states.

For the HT800 sample, there is a clear π^* feature at 285 eV, whereas the spectrum observed over the following 20 eV is smooth and featureless, typical of an amorphous carbon. For the HT200 sample, the relative π^* peak intensity is much greater and the σ^* structure is clearly more defined. At higher energies (\sim 330 eV) there is also a weaker feature arising from a multiple scattering resonance (MSR) [24]. This provides evidence that the structure is becoming more ordered with increasing HTT.

In the low loss spectra, the HT2000 sample has a plasmon peak at ~ 6.5 eV and a large, broad peak at 24 eV corresponding to transitions between the π and π^* states. These peaks are also seen in graphitised carbon, although they are shifted to higher energies for crystalline graphite. [25]



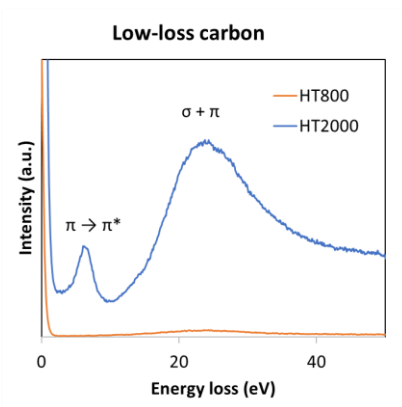


Fig 5. EELS Spectra for HT800 (orange trace) and HT2000 (blue trace): (a) carbon K-edges (coreloss) and (b) low-loss region. Note the change in the π^* peak intensity, the increased detail in the σ^* region and the shift in the multiple scattering resonance (MSR) peak as temperature increases.

			<u> </u>
Sample	1s $ ightarrow$ π* (C-C)	1s →σ* (C- H)	1s →σ* (C- C)
HT800	285.6	287.9	292.0
HT2000	285.6	287.8	292.6

Table 1. Peak positions in the EELS spectra

It is possible to determine the relative amounts of π and σ -bonded carbon from the relative intensities of the $1s\to\pi^*$ and $1s\to\sigma^*$ features in the near-edge structure. To estimate the relative amounts, it is assumed that the ratio of integrated areas under the π^* peak and the σ^* peak is proportional to Nsp2/Nsp3. The respective areas are obtained by applying a Gaussian fit to the spectra and integrating the respective curves at ~285 and 292 eV. The ratio of this π^* peak intensity to the total C K-edge intensity is then taken – the total intensity (I_{tot}) usually being measured in a window of up to 20 eV extending from the edge onset and covering both the π^* peak and the majority of the subsequent $1s\to\sigma^*$ structure. The intensity ratio, (I_{π^*}/I_{tot}), is proportional to the fraction of the total carbon atoms in the material involved in π bonding, however, this needs to be normalised to a reference spectrum containing 100% sp2 bonding, e.g. highly oriented pyrolytic graphite. The normalised intensity ratio can then be used to obtain the sp2 fraction, provided that the different carbon bonding states are known, e.g. just sp2 and sp3.

The peak positions of the features of the EELS spectra are summarised in Table 1. Four Gaussian curves were fitted to the data: G1 centered at \sim 285 eV for the C=C $\pi*$ component; G2 \sim 292 eV, the C=C $\sigma*$ component and G3 \sim 300 eV, the C=C $\sigma*$ component. Peaks were partially constrained in terms of peak position and widths according to [24]. The additional Gaussian peak was positioned under the "residual" peak (\sim 286–288 eV) described in Zhang's paper. [24] This peak is either from the presence of additional atoms (e.g. O or H) or non-planar sp2-bonded (fullerene-like) carbon components.

The energy windows integrated for the π^* and σ^* peak areas were determined according to Berger and McKenzie [25]. In order for the Sp2/Sp3 content to be calculated, the ratio obtained will need to be normalised to the ratio observed within a spectrum obtained from a 100% sp2 hybridized material (e.g. a perfect graphite crystal). This is part of future work.

Daniels et el. [26] have also demonstrated that the C–C bond length may be deduced from the peak position of the multiple scattering resonance at the C K-edge which appears at ~330 eV, with an accuracy of 0.1 pm. Analysis of this peak will be carried out in future analyses.

2.4 Raman Spectroscopy

The normalized first-order Raman spectra for the PF resin and heat-treated samples are shown in Figure 6, ordered from bottom to top according to increasing HTT. The spectral range from 800 to 3000 cm⁻¹ for all samples show two main peaks at approximately 1300 and 1580-1600 cm⁻¹ corresponding to the disorder-induced, D, and graphitic, G, bands, respectively. These are characteristic features of carbon materials and are directly linked to the vibrational modes of the sp2 bonds. The G band arises from the in-plane stretching modes of pairs of sp2-bonded carbon atoms, and its peak position can vary from 1500 to 1630 cm⁻¹. [27] The D band intensity is connected to the breathing modes of sixfold aromatic rings and requires a defected structure to become Raman active. [27] This mode is, therefore, absent in highly crystalline graphite.

Analysis of these peaks can provide a wealth of structural information. Shifts and line-width variations of the G band are indications of the defects in the lattice.

The Raman spectra were fitted with Lorentzian and Gaussian line shapes using the Fityk software. A representative example of the fitting is shown for HT2800 and HT1200 samples in Fig 6. As a result of the peak fitting, we can distinguish the presence of weak D3 and D4 bands. This is consistent with the raman spectra of glassy carbons reported in the literature. Five components contribute to the first-order Raman spectrums: (1) graphitic G peak at 1579 cm⁻¹ (2) disordered D1 peak at 1304 cm⁻¹, (3) D2 peak at 1609 cm⁻¹ (appears more clearly for the highest temperature sample) (4) D3 peak at 1535 cm⁻¹, (5) D4 peak at 1168 cm⁻¹ (which weakens in intensity during the progressive heat treatment). Although a fifth (D5) peak has been reported in the literature, we did not find the presence of this peak in our samples.

As is the case with XRD reflections, Raman bands sharpen and their FWHM values decrease as the heat-treatment temperature increases. At the lower HTT these peaks are broad and overlapping. The intensity of the also G band increases with respect to the D band up to 2800 °C. At the highest HTTs of 2600 and 2800 °C, the D2 and 2D1 bands also become much sharper.

The FWHM of the G band correlates with structural disorder, and the G band position shifts with the degree of graphitization upon increasing HTT. As the layer thickness increases, the band position shifts to lower energy, from 1593 to 1579 cm⁻¹, and the FWHM decreases.

The D band position for graphite is located around 1360 cm⁻¹ however, in our results, the D peak appears at a significantly lower energy, around 1300 cm⁻¹. It is known that both the position and the shape of the band can vary significantly with different excitation laser frequencies, however further analysis is required to understand this peak shift.

The mathematical formula, known as the T-K rule, states that the ratio of the integrated intensities of the D to G bands, I(D)/I(G), is inversely proportional to the interplanar length of the graphitic domains (La). This can be used to determine the extent of graphitization with increasing HTT. [28]

 $I(D)/I(G) = C(\lambda)/La$, where $C(\lambda)$ is a constant for a given laser beam wavelength.

Based on this rule, the I(D)/I(G) ratio should decrease with increasing HTT as the carbon structure becomes more ordered. The data here show that I(D)/I(G) increases up to 1800 °C and then rapidly decreases up to 2800 °C. This is in contrast to the trend reported by Jurkiewicz *et al.* [29], whose data show that I(D)/I(G) increases with pyrolysis temperature.

Interestingly, Fujimori *et al* [30] experimentally identified a Raman signal from STW defects on single-walled carbon nanotubes in the range of $1100-1200~\rm cm^{-1}$. The D4 peaks observed in these results could also come from the vibrations of carbon atoms in non-hexagonal rings such as STW defects which are considered as the reason of the fullerene-like structure of glassy carbons.

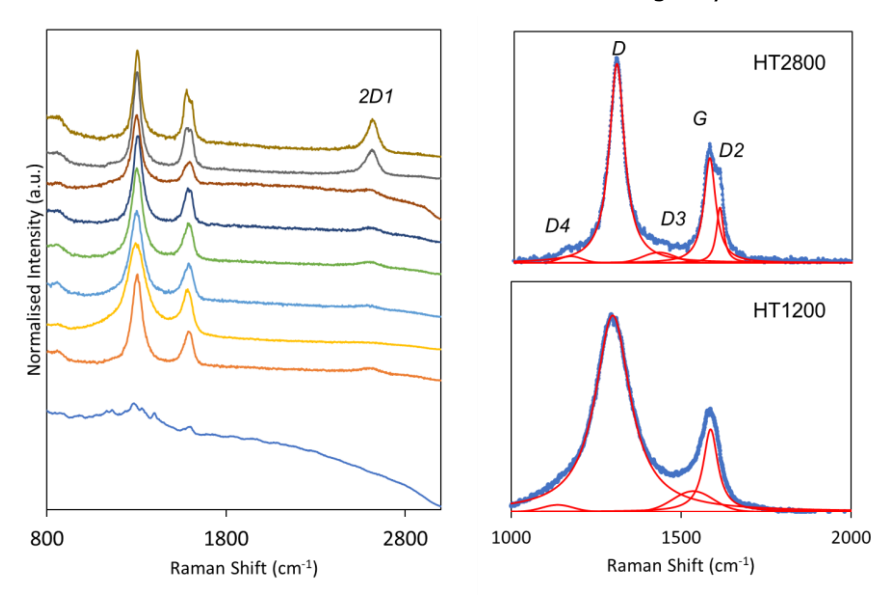


Fig 6. Raman spectra (normalised intensity); PF resin (bottom blue trace) and disordered carbons at increasing HTTs from 600-2800 °C (HT600-HT280 bottom to top trace). Peak fitting showing the best fit to the experimental data for HT2800 and HT1200. The D, G and D2 bands are fit

with Lorentzian peaks, whilst the D3 and D4 bands are fit with broad Gaussians. The D band becomes narrower and the D2 and 2D1 bands appears with increasing HTT.

2.5 SAXS

Figure 7 shows preliminary results from SAXS experiments carried out on the I22 beamline at DLS. An initial assessment of the data shows there is a marked change in the SAXS profiles for the heat-treatment samples at temperatures above 1200 °C. Future work will involve fitting SAXS data with appropriate models for the pores using the SASView software package. Figure 7 also shows an SEM (Zeiss Sigma 360 VP) of the surface morphology of a particle of HT2800 produced by automated ball milling. There is evidence of nanoporosity as well as a spherical morphology which may arise due to the presence of curved nano structures that have been reported in disordered carbons heat treated to 2800 °C. Further work is required to correlate the SEM images with that of the SAXS and ptychography data to quantify the form of the closed porosity.

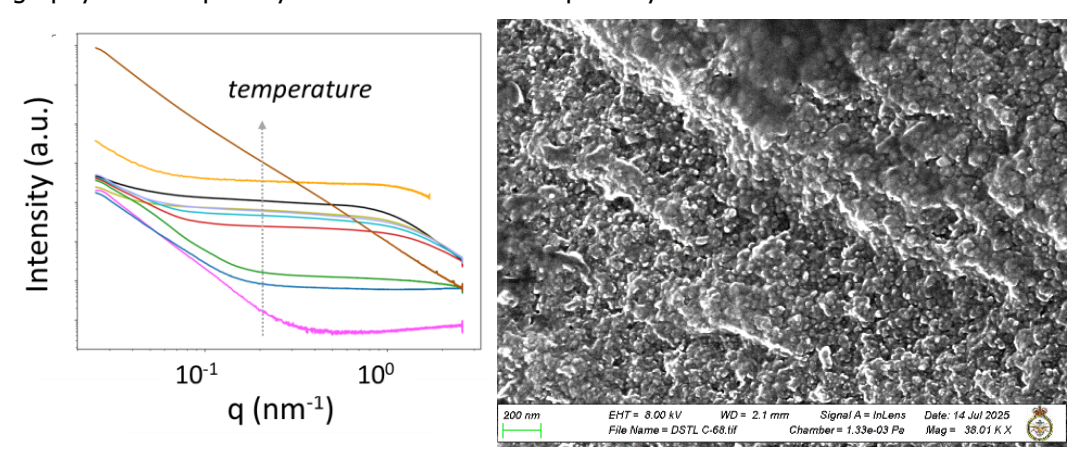


Fig 7. (a) SAXS data: Traces from bottom to top with increasing HTT. A commercial VC sample is shown in yellow and isotropic graphite in brown for comparisons. (b) SEM image for HT2800 powdered sample at a 38k magnification. The scale bar is 200 nm.

3. Conclusions

The disordered carbons produced by pyrolysis of phenol-formaldehyde resins at increasing temperatures from 600 °C up to 2800 °C have been thoroughly characterised using a number of advanced techniques; wide and small-angle x-ray scattering, Raman spectroscopy, electron energy loss spectroscopy, scanning electron microscopy, elemental analysis and ptychography. The results presented are consistent with those in the literature for NGCs. Sp2-hybridised carbons are arranged in discrete graphene sheets that stack randomly to form nanometer-sized domains. These small, coherent domains increase in size with HTT, but the long-range structures are still disordered, and are not re-organised into crystalline graphite, even at the highest temperature of 2800 °C. The results also revealed that inter-layer correlations, *Lc*, are short-ranged and less affected by the HTT heat-treatment temperature than intra-layer correlations, *La*, indicating that lateral growth is more favorable.

More research is needed to determine the arrangement of atoms in detail and to understand the relationship between the atomic scale structure and physical properties. It is anticipated that future analysis of data collected from SAXS, ptychography and CDI experiments, in combination with theoretical modelling, will provide further insight into the nanoporosity and micro-structural evolution of these materials as a function of HTT. Further work will also consider the chemistry of the precursor material and the possible origin of non-hexagonal rings in NGC and their role in impeding graphitization, even at temperatures as high as 3000 °C. The presence of non-planar nanocarbons, such as fullerenes, may also explain the origin of the microporosity.

By combining both experimental and theoretical methods, we also plan to produce atomistic models of disordered carbons as a function of HTT which will enable the calculation of thermal properties to further our understanding of structure-property relationships.

References

- 1. Schmidt, D.L.: Ablative Polymers in Aerospace Technology, Journal of Macromolecular Science: Part A Chemistry, 3:3, 327-365 (1969)
- 2. Tzeng, S.; Chr, Y.: Evolution of microstructure and properties of phenolic resin-based carbon/carbon composites during pyrolysis, Materials Chemistry and Physics, 73, 2-3, 162-169, (2002). https://doi.org/10.1016/S0254-0584(01)00358-3
- 3. Monthioux, M.: Describing Carbons, Carbon Trends, 14, 100325 (2024). https://doi.org/10.1016/j.cartre.2024.100325
- 4. Franklin R.E.: Crystallite growth in graphitizing and non-graphitizing carbons. Proc. R. Soc. Lond. A, 209, 196–218 (1951). https://doi.org/10.1098/rspa.1951.0197
- 5. Warren, B.E.: X-ray diffraction in random layer lattices, Phys. Rev., 59, 693-698 (1941). https://doi.org/10.1103/PhysRev.59.693
- 6. Oberlin, A. Carbonization and graphitization, Carbon, 22, 521–541 (1984). https://doi.org/10.1016/0008-6223(84)90086-1
- 7. Oberlin, A.: High resolution TEM studies of carbonization and graphitization, Chem. Phys. Carbon, 22 (1989)
- 8. Jenkins, G.M.; Kawamura, K.: Structure of glassy carbon. Nature, 231, 175–176 (1971).
- 9. Harris, P. J. F.; Tsang, S. C.: High-resolution electron microscopy studies of non-graphitizing carbons. Philosophical Magazine A, 76(3), 667–677 (1997). https://doi.org/10.1080/01418619708214028
- 10. Kroto, H.W.; Heath, J.R.; O'Brien, S.C.; Curl, R.F.; Smalley, R.E.: C₆₀: Buckminsterfullerene, Nature, 318, 162-163 (1985). https://doi.org/10.1038/318162a0
- 11. Ugarte, D.: Curling and closure of graphitic networks under electron-beam irradiation, Nature, 359, 707–709 (1992). https://doi.org/10.1038/359707a0
- 12. Iijima, S.: Helical microtubules of graphitic carbon, Nature, 354, 56–58 (1991). https://doi.org/10.1038/354056a0
- 13. Basham, M.; Filik, J.; Wharmby, M.T.; Chang, P.C.Y.; El Kassaby, B.; Gerring, M.; Aishima, J.; Levik, K.; Pulford, B.C.A.; Sikharulidze, I. *et al.*: J. Synchrotron Rad. 22 (2015). doi:10.1107/S1600577515002283
- 14. Soper, A.; Data reduction for neutron and x-ray scattering experiments (2021) https://github.com/disorderedmaterials/Gudrun
- 15. Granlund, L.; Billinge, S. J. L. and Duxbury, P.M.: Algorithm for systematic peak extraction from atomic pair distribution functions, Acta Crystallogr. A 4, 392-409 (2015)
- 16. Wojdyr, M.: Fityk: a general-purpose peak fitting program, J. Appl. Cryst. 43, 1126-1128 (2010)
- 17. Doucet, M. et al. SasView Version 5.0.6, Zenodo, 10.5281/zenodo.7581379
- 18. Perret, R.; Ruland, W.: X-ray small-angle scattering of glassy carbon. J. Appl. Cryst., 5, 183-187, (1972). https://doi.org/10.1107/S0021889872009161
- 19. Osswald, O.; Smarsly, B.M. OctCarb—A GNU Octave Script for the Analysis and Evaluation of Wide-Angle Scattering Data of Non-Graphitic Carbons. C, 8, 78 (2022). https://doi.org/10.3390/c8040078
- 20. Uskoković, V.: A historical review of glassy carbon: Synthesis, structure, properties and applications, Carbon Trends, 5, 100116 (2021). https://doi.org/10.1016/j.cartre.2021.100116
- 21. Badaczewski, F.; Loeh, M.O.; Pfaff, T.; Dobrotka, S.; Wallacher, D; Clemens, D; Metz, J.; Smarsly, B.M.; Peering into the structural evolution of glass-like carbons derived from phenolic resin by combining small-angle neutron scattering with an advanced evaluation

- method for wide-angle X-ray scattering, Carbon, 141, 169-181, (2019). https://doi.org/10.1016/j.carbon.2018.09.025
- 22. Osswald, O.; Loeh, M.O.; Badaczewski, F.M.; Pfaff, T.; Fischer, H.E.; Franz, A.; Hoffmann, J.-U.; Reehuis, M.; Klar, P.J.; Smarsly, B.M.; On the Highly Ordered Graphene Structure of Non-Graphitic Carbons (NGCs)—A Wide-Angle Neutron Scattering (WANS) Study. Journal of Carbon Research C 9, 27, (2023). https://doi.org/10.3390/c9010027
- 23. Jurkiewicz, K.; Duber, S.; Fischer, H. E.; Burian, A.: Modelling of glass-like carbon structure and its experimental verification by neutron and X-ray diffraction. Journal of Applied Crystallography, 50, (2017). https://doi.org/10.1107/S1600576716017660
- 24. Zhang, Z.L.; Brydson, R.; Aslam, Z.; Reddy, S.; Brown, A.; Westwood, A.; Rand, B.: Investigating the structure of non-graphitising carbons using electron energy loss spectroscopy in the transmission electron microscope, Carbon, 49, 5049–5063, (2011). https://doi.org/10.1016/j.carbon.2011.07.023
- 25. Berger S.D.; McKenzie, D.R.; Martin, P.J.: EELS analysis of vacuum arc-deposited diamond-like films. Philos Mag Lett, 57, 285–290 (1988). https://doi.org/10.1080/09500838808214715
- 26. Daniels, H.; Brydson, R.; Rand, B.; Brown, A.: Investigating carbonization and graphitization using electron energy loss spectroscopy (EELS) in the transmission electron microscope (TEM), Philos Mag, 87, 4073–4092, (2007). https://doi.org/10.1080/14786430701394041
- 27. Ferrari, A. C.; Robertson, J.: Interpretation of Raman spectra of disordered and amorphous carbon. Physical review B, 61(20), 14095 (2000)
- 28. Tuinstra, F.; Koenig, J. L.: Raman spectrum of graphite, The Journal of Chemical Physics, 53(3), 1126-1130 (1970)
- 29. Jurkiewicz, K. *et al*; Evolution of glassy carbon under heat treatment: correlation structure—mechanical properties, J Mater Sci, 53, 3509–3523 (2018)
- 30. Fujimori, T.; Radovic, L. R.; Silva-Tapia, A. B.; Endo, M.; Kaneko, K.: Structural importance of Stone—Thrower–Wales defects in rolled and flat graphenes from surface-enhanced Raman scattering, Carbon, 50(9), 3274-3279 (2012)

Acknowledgements

We acknowledge Diamond Light Source for time on Beamlines I15-1, I22 and I13-1 and the ePSIC instruments E01 and E03 under the following proposal numbers: CY34534-1, SM37118-1, SM39025-1, CY39478-1, MG40242, MG40841/2.

We also acknowledge Mr David Hartley, Defence Science and Technology Group (DSTG), for assistance with sample preparations, Mr David Pearson, 1710 Naval Air Squadron (NAS), for SEM imaging and elemental analysis and Clare Nixon (Dstl) for the Raman spectroscopy.

Copyright Statement

The contents include material subject to © Crown copyright (2025), Dstl. This information is licensed under the Open Government Licence v3.0. To view this licence, visit

Where we have identified any third party copyright information you will need to obtain permission from the copyright holders concerned. Any enquiries regarding this publication should be sent to: centralenquiries@dstl.gov.uk

HiSST-2025-185
Determining the Atomic Arrangement of Disordered Carbon